NUMERICAL STUDY OF THE RESULTANT SEDIMENT TRANSPORT NEAR THE PORT OF NGQURA DUE TO THE BLOCKAGE OF A SEDIMENT BYPASS SYSTEM

Baloyi J.*, Mahlathi C.D., Wessels G.J.C., Ubbink O. and Smit J.E.
*Author of correspondence
Modelling and Digital Science, Council for Scientific and Industrial Research,
Pretoria, 0001,
South Africa,
E-mail: jbaloyi@csir.co.za

ABSTRACT

The Port of Ngqura, situated in the Algoa Bay of South Africa, was commissioned in 2009 together with a sediment bypass system that is meant to intercept sediment being transported naturally eastwards towards the entrance of the port. The sea state in the Algoa Bay is dominated by waves generated in the Southern Ocean and flow from the Agulhas Current as it flows westwards along the southern coastline of South Africa. This sea state results in waves with an average significant wave height of more than 2 m over all seasons of the year. The sediment bypass system got blocked by rock fragments and stones migrating into the sediment trap created to accommodate eduction pumps sucking the fluidised sediment onshore for pumping downstream, to the right of the eastern breakwater. This resulted in the need for regular dredging in order to keep the entrance channel into the port open. The resulting sediment transport that necessitated the dredging operation was studied numerically by using the Delft3D software code. Delft3D Flow with its morphology module was coupled with Delft3D SWAN (Simulating WAves Nearshore) in stationary mode where data from National Centre for Environmental Prediction (NCEP) averaged over a 3 hour period was used as input for wave and wind data. Two nested grids were used to compute the wave propagations using SWAN where the larger grid took input of significant wave height, peak wave period and wave direction from NCEP, and it had a grid resolution of about 1000 m. The smaller inner grid (which had a resolution of about 500 m) got its boundary inputs from the calculated solution of the larger grid. All the wave conditions for SWAN were implemented with a directional spreading of 25 degrees with the JONSWAP shape. Thin dams were used to model the breakwaters of ports in the model and small islands. The influence of the Agulhas current was approximated by a current with a magnitude of 0.2 m/s and a direction of 250 degrees. Boundary conditions input into the Delft3D Flow model were water level computed using an in-house code that took current, wind and water level as input to calculate the water level at the right boundary node. The water level solution from Delft3D-Flow was used as input to the SWAN models. The bed and suspended sediment transport terms were computed over a period of 6 months, and compared to discern dominant processes responsible for the migrating stones, rock fragments and sediment filling up the bypass system sediment trap.

INTRODUCTION

The Port of Ngqura, situated in the Algoa Bay of South Africa, was commissioned in 2009 together with a sediment bypass system that is meant to intercept sediment being transported naturally eastwards towards the entrance of the port. The sea state in the Algoa Bay is dominated by waves generated in the Southern Ocean and flow from the Agulhas Current as it flows westwards along the southern coastline of South Africa as illustrated in Figure 1.

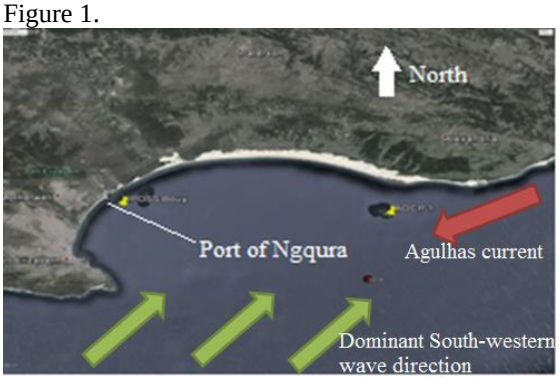

Figure 1 Google Earth Image of Algoa bay showing locations of measuring instruments, and direction of the Agulhas current dominant wave direction.

This sea state results in waves with an average significant wave height of more than 2 m over all seasons of the year. Schumann and Brink [1] found that coastal trapped waves have occasional amplitudes in excess of 0.5 m along the south coast of South Africa. This partly contributes to the findings by Goschen et al. [2] that the Algoa Bay water level variations were a combination of wind, wave setup, tidal variations and trough activity of the coastal trapped waves. In Algoa Bay the coastal ocean currents that flow either eastwards or westwards are aligned to the prevailing winds as measured by Roberts [3]. It was also found that at the 17.5 m contour just off the eastern breakwater of the Port of Ngqura the response of the currents to winds was rapid (in the order of 2-7 hours) (Roberts [3] and Lwandle [4]). Velocities of currents were measured to be 0.5 m/s at the seafloor and exceed 1 m/s on the water surface. Goschen et al. [2] found that currents around Cape Padrone can switch to downwind direction during north-eastern winds, causing coastal sea-level drop. Roberts [3] reported that currents in the bay can run counter to the wind for long periods (approximately 45 days). This is due to the Ekman veering in the bottom boundary layer of the Agulhas current near Bird Island according to Goschen et al. [2]. Nearshore zone near Port of Ngqura is dominated by wave-driven currents, which can be of significant magnitude under high wave conditions. Because of the obstruction by the Port of Ngqura of the alongshore flow, there resulted recirculation zones are NE of the eastern breakwater and SW of the western breakwater. Current speeds 500 m offshore are greatest in spring and summer, and least in autumn and lowest in winter when the water column is well mixed. In the nearshore zone the currents are the strongest in winter and spring. Goschen et al. [2] has identified the Ekman veering as being responsible for transporting bottom water to the surface, resulting in south-westward flowing surface currents around Bird Island. Wind-driven upwelling and downwelling was found to be present at Woody Cape at first and then moves north-eastwards towards Port Alfred. This movement follows the same anti-clockwise pattern of the weather systems around the coast of South Africa ([2]). In addition Goschen and Schumann [5] found that the upwelling at Cape Recife, along the southern shoreline, is predominantly generated by wind, while wind and the Agulhas Current influence the upwelling at Cape Padrone. South African tides are semidiurnal microtidal, which means that there are two high tides and two low tides per day. There is a significant tidal range from a neap tide of 0.5 m to a spring tide of 2 m.

The Algoa Bay region is dominated by winds that are either west-southwesterly or east-southeasterly , which are orientated parallel to the large scale orientation of the coastline (Schumann and Martin [6] and Goschen and Schumann [7]). The west-southwesterly winds are dominant most times of the year, whereas the east-southeasterly dominant between seasons.

NOMENCLATURE

a	[m]	reference height
$c^{(l)}$	[kg/m^3]	mass concentration of sediment fraction (l)
$c_a^{(l)}$	[kg/m^3]	mass concentration at reference height a
c_x	[m/s]	propagation velocity in the x-space
c_y	[m/s]	propagation velocity in the y-space
c_σ	[m/s]	propagation velocity in the σ-space
c_θ	[m/s]	propagation velocity in the θ - space
$D_*^{(l)}$	[-]	non-dimensional particle diameter
$D_s^{(l)}$	[m]	representative diameter of suspended sediment
d	[m]	water depth below the reference plane
E	[-]	energy density spectrum
f	[1/s]	Coriolis parameter
F_ξ	[m/s^2]	turbulent momentum flux in the ξ direction
F_η	[m/s^2]	turbulent momentum flux in the η direction
g	[m/s^2]	gravitational acceleration
$\sqrt{G_{\xi\xi}}$	[-]	coefficient used to transform curvilinear to rectangular coordinates
$\sqrt{G_{\eta\eta}}$	[-]	coefficient used to transform curvilinear to rectangular coordinates
H	[m]	total water depth
M_ξ	[m/s^2]	sources or sinks of momentum in the ξ direction
M_η	[m/s^2]	sources or sinks of momentum dη direction
M	[-]	the sediment mobility number due to waves and currents
M_e	[-]	excess sediment mobility number
N	[-]	action density spectrum
P	[kg/ms^2]	hydrostatic pressure
P_{atm}	[kg/ms^2]	atmospheric pressure of air

P_ξ	[kg/m^{2}s^2]	gradient hydrostatic pressure in the ξ direction
P_η	[kg/m^{2}s^2]	gradient hydrostatic pressure in the η direction
Q	[m/s]	global source or sink term per unit area
q_{in}	[1/s]	local sources of water per unit volume
q_{out}	[1/s]	local sinks of water per unit volume
S_b	[kg/ms]	bedload sediment transport
S	[-]	source term
$T_a^{(l)}$	[-]	non-dimensional bed shear tress
t	[s]	time
U	[m/s]	depth averaged velocity component
u	[m/s]	instantaneous velocity component
U_{on}	[m/s]	near-bead peak orbital velocity in onshore direction based on the significant wave height
V	[m/s]	depth averaged velocity component
v	[m/s]	instantaneous velocity component
v_{eff}	[m/s]	effective velocity
v_{cr}	[m/s]	critical depth averaged velocity for initiation of motion
v_R	[m/s]	magnitude of an equivalent depth averaged velocity computed from the velocity in the bottom computational layer
$w_s^{(l)}$	[m/s]	hindered sediment settling velocity of sediment (l)
w	[m/s]	instantaneous velocity vertical component
x	[m]	horizontal Cartesian co-ordinate component
y	[m]	horizontal Cartesian co-ordinate component
z	[m]	vertical co-ordinate in physical space

Special characters

$\varepsilon_{s,x}^{(l)}$	[m^2/s]	eddy diffusivity component of sediment fraction (l)
$\varepsilon_{s,y}^{(l)}$	[m^2/s]	eddy diffusivity component of sediment fraction (l)
$\varepsilon_{s,z}^{(l)}$	[m^2/s]	eddy diffusivity component of sediment fraction (l)
η	[-]	horizontal curvilinear coordinate
ν_V	[m^2/s]	vertical eddy viscosity
ρ_0	[kg/m3]	reference density of water
ρ	[kg/m^3]	density of water.
$\rho_s^{(l)}$	[kg/m^3]	density of the sediment particle
σ	[1/s]	relative frequency
θ	[Rad]	wave direction normal to the wave crest of each spectral component
ζ	[m]	free surface elevation above the reference plane (at $z = 0$)
ξ	[-]	horizontal curvilinear coordinate

The sediment bypass system got blocked by rock fragments and stones migrating into the sediment trap created to accommodate eduction pumps sucking the fluidised sediment onshore for pumping downstream, to the right of the eastern breakwater. This resulted in the need for regular dredging in order to keep the entrance channel into the port open. The resulting sediment transport that necessitated the dredging operation was studied numerically by using the Delft3D software code.

METHOD

For the purpose of the present study, the wind and wave conditions were defined by a numerical forecast offshore data set covering a period about of 15 years. This data set is based on the daily forecasts from the National Centre for Environmental Prediction (NCEP), a sub-division of the USA based National Oceanic Atmospheric Administration group. The NCEP data covers the entire offshore region of the SA coastline. This data set was employed by (Theron et al. [8]). Wave conditions and the flow conditions experienced by the region of the Algoa Bay under investigation were modelled on two separate numerical model grids using two different modules as implemented in the numerical code Delft3D, namely: SWAN and Delf3D-FLOW. The two modules used to solve the wave and flow conditions were coupled in an iterative manner. The wave spectrum solution was first coupled with the flow model to simulate the wave induced currents. The water levels solution from the flow model would then be coupled to the wave module for the next iteration, through a water level correction in the wave computation. The

communication between the models were executed every 3 hours of simulated time during the simulation run time, this corresponded to the wave boundary condition updates obtained from NCEP. The wave conditions were modelled using the SWAN module ([9]), which implements a time series of wave conditions from the offshore NCEP wave spectrum. The model wind field was also inferred from NCEP and applied to both the WAVE and FLOW ([10]) models as a uniform wind field. The flow boundary conditions were forced using tidal astronomic constituents, causing water level fluctuations. A constant background current of 0.2 m/s, simulating the Agulhas Current, was also applied to the flow boundary conditions together with the water level changes caused by offshore and nearshore wind conditions.

Flow modelling

The flow condition solutions were computed by using the curvilinear grid presented in Figure 2. The smallest grid cell resolution was less than 100 m. The resolution of the present flow grid increased in resolution from the off-shore to the nearshore.

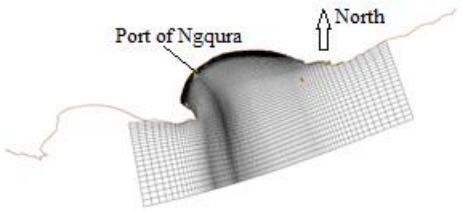

Figure 2 Curvilinear flow grid for the Algoa Bay numerical model.

In the flow model the details of the Port of Ngqura and Port Elizabeth, as seen in Figure 3, were simplified by using dry points to represent regions that are dry and thin dams to represent the breakwaters. The above mentioned are numerical tools used to restrict the numerical flow computation from areas and regions were no fluid motion should be taking place.

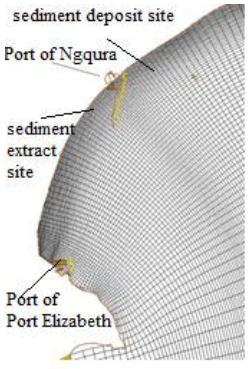

Figure 3 Close up of the flow grid model showing simplifications made to the Port of Ngura and old Port of Port Elizabeth.

The vertical grid in Delft3D-FLOW discretised using the σ co-ordinate system where grid layers follow the bottom topography and the free surface, whereby a smooth representation of the topography is obtained. The σ co-ordinate system is defined as: $\sigma = \frac{z-\zeta}{H} = \frac{z-\zeta}{d+\zeta}$ (1)

Where z is the vertical co-ordinate in physical space; ζ is the free surface elevation above the reference plane (at $z=0$); d is the water depth below the reference plane, and H is the total water depth. Therefore $\sigma=-1$ at the bottom of the ocean and $\sigma=0$ on the sea surface. The depth-averaged continuity equation is used to represent the conservation of an incompressible fluid as given by equation (2).

$$\frac{\partial\zeta}{\partial t}+\frac{1}{\sqrt{G_{\xi\xi}}\sqrt{G_{\eta\eta}}}\frac{\partial\left((d+\zeta)U\sqrt{G_{\eta\eta}}\right)}{\partial\xi}+\frac{1}{\sqrt{G_{\xi\xi}}\sqrt{G_{\eta\eta}}}\frac{\partial\left((d+\zeta)V\sqrt{G_{\xi\xi}}\right)}{\partial\eta}=(d+\zeta)Q \quad (2)$$

Where U and V are the depth averaged velocities expressed, respectively as; $\sqrt{G_{\xi\xi}}$ and $\sqrt{G_{\eta\eta}}$ are coefficients used to transform curvilinear to rectangular coordinates; $Q=\int_{-1}^{0}(q_{in}-q_{out})d\sigma$ is a global source or sink term per unit area, q_{in} and q_{out} are the local sources and sinks of water per unit volume respectively; ξ and η are the horizontal curvilinear coordinates; u and v are the instantaneous velocities. The momentum equation in the ξ horizontal curvilinear coordinate is given by:

$$\frac{\partial u}{\partial t}+\frac{u}{\sqrt{G_{\xi\xi}}}\frac{\partial u}{\partial\xi}+\frac{v}{\sqrt{G_{\eta\eta}}}\frac{\partial u}{\partial\eta}+\frac{w}{d+\zeta}\frac{\partial u}{\partial\sigma}-\frac{v^2}{\sqrt{G_{\xi\xi}}\sqrt{G_{\eta\eta}}}\frac{\partial\sqrt{G_{\eta\eta}}}{\partial\xi}+\frac{uv}{\sqrt{G_{\xi\xi}}\sqrt{G_{\eta\eta}}}\frac{\partial\sqrt{G_{\xi\xi}}}{\partial\eta}-fv=-\frac{1}{\rho_0\sqrt{G_{\xi\xi}}}P_\xi+F_\xi+\frac{1}{(d+\zeta)^2}\frac{\partial}{\partial\sigma}\left(\nu_V\frac{\partial u}{\partial\sigma}\right)+M_\xi \quad (3)$$

The momentum equation in the η horizontal curvilinear coordinate has the same form as equation (3), and will not be shown for brevity.

Where w is the vertical velocity; f is the Coriolis parameter; ρ_0 is the reference density of water (1024 kg/m^3); P_ξ and P_η are the gradient hydrostatic pressures in the ξ and η directions respectively; F_ξ and F_η are the turbulent momentum fluxes in the ξ and η directions respectively; M_ξ and M_η are the sources or sinks of momentum in the ξ and η directions respectively; ν_V is the vertical eddy viscosity. The vertical velocity w in the σ-coordinate system is calculated from the continuity equation. The shallow water assumption was used to reduce the vertical velocity equation to a hydrostatic pressure equation given by: $P = P_{atm} + gH\int \rho(\xi,\eta,\sigma',t)d\sigma'$. Where P is the hydrostatic pressure; P_{atm} is the atmospheric pressure of air; g is the gravitational acceleration; ρ is the density of water.

Sediment transport modelling

Sediment transportation was modelled by looking at suspended sediment and bedload sediment. Suspended sediment transport was modelled as expressed by equation (4).

$$\frac{\partial c^{(l)}}{\partial t} + \frac{\partial uc^{(l)}}{\partial x} + \frac{\partial vc^{(l)}}{\partial y} + \frac{\partial\left(w - w_s^{(l)}\right)c^{(l)}}{\partial z} - \frac{\partial}{\partial x}\left(\varepsilon_{s,x}^{(l)}\frac{\partial c^{(l)}}{\partial x}\right) - \frac{\partial}{\partial y}\left(\varepsilon_{s,y}^{(l)}\frac{\partial c^{(l)}}{\partial y}\right) - \frac{\partial}{\partial z}\left(\varepsilon_{s,z}^{(l)}\frac{\partial c^{(l)}}{\partial z}\right) = 0 \quad (4)$$

Where: $c^{(l)}$ is the mass concentration of sediment fraction (l); $\varepsilon_{s,x}^{(l)}, \varepsilon_{s,y}^{(l)}$ and $\varepsilon_{s,z}^{(l)}$ are the eddy diffusivities of sediment fraction (l); $w_s^{(l)}$ is the hindered sediment settling velocity of sediment (l). The settling velocity of the sediment fraction was calculated as given by equation (5).

$$w_s^{(l)} = \frac{10\nu}{D_s^{(l)}}\left(\sqrt{1 + \frac{0.01\left(\rho_s^{(l)}/\rho - 1\right)gD_s^{(l)3}}{\nu^2}} - 1\right) \quad (5)$$

Where: $D_s^{(l)}$ is the representative diameter of suspended sediment (in this study 200 μm is used; $\rho_s^{(l)}$ is the density of the sediment particle. There is a reference height a above which sediment in the water column was considered suspended, thereby entrained in the water column. The reference mass concentration computed at the reference height is as expressed in equation (6).

$$c_a^{(l)} = 0.015\rho_s^{(l)}\frac{D_{50}^{(l)}\left(T_a^{(l)}\right)^{1.5}}{a\left(D_*^{(l)}\right)^{0.3}} \quad (6)$$

Where: $c_a^{(l)}$ is the mass concentration at reference height a; $D_*^{(l)}$ is the non-dimensional particle diameter; $T_a^{(l)}$ is the non-dimensional bed shear tress. The magnitude of the bedload sediment transport was computed as: $|S_b| = 0.006\rho_s w_s D_{50}^{(l)} M^{0.5} M_e^{0.7}$; Where: S_b is the bedload sediment transport; M is the sediment mobility number due to waves and currents, and M_e is the excess sediment mobility number; $v_{eff} = \sqrt{v_R^2 + U_{on}^2}$; v_{cr} is the critical depth averaged velocity for initiation of motion; v_R is the magnitude of an equivalent depth averaged velocity computed from the velocity in the bottom computational layer; U_{on} is the near-bead peak orbital velocity in onshore direction based on the significant wave height.

Wave modelling

The wave conditions were computed by using two grid models as shown in Figure 4. The bigger grid has a grid resolution of 1000m and the input water level values at the open boundaries were taken from NCEP point 32565. The smaller grid model had a grid resolution of 500m and its input at the boundaries was from the computed solution from the big grid model.

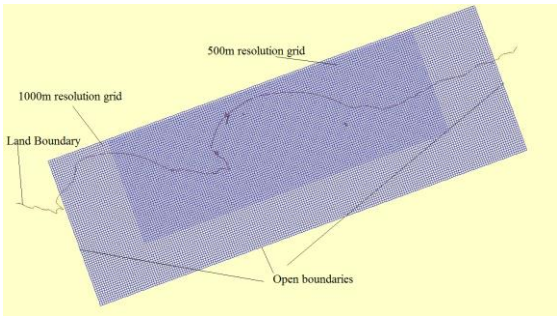

Figure 4 Wave grid models with 1000m and 500m grid resolutions for the Algoa Bay model.

Delft3D SWAN models wave interaction and propagation through the water by means of an action density spectrum $N(\sigma,\theta)=\frac{E(\sigma,\theta)}{\sigma}$, which takes into account wave current interaction. Where E is the energy density spectrum; σ is the relative frequency; and θ is the wave direction normal to the wave crest of each spectral component. SWAN models the evolution of the wave spectrum by means of a spectral action balance equation as expressed in equation (7).

$$\frac{\partial}{\partial t}N+\frac{\partial}{\partial x}c_x N+\frac{\partial}{\partial y}c_y N+\frac{\partial}{\partial \sigma}c_\sigma N+\frac{\partial}{\partial \theta}c_\theta N=\frac{S}{\sigma} \quad (7)$$

Where t is time; x and y are the horizontal Cartesian co-ordinates; c_x and c_y are the propagation velocities in the x-and y-space respectively; The fourth term represents the shifting of the relative frequency due to changes in depths and currents, and it propagates at the velocity c_σ in σ-space; The fifth term stands for the current-induced and depth-induced refraction, which propagates at the velocity c_θ in θ- space; The source term $S(\sigma,\theta)$ at the right hand side of equation (7) takes into account the effects of non-linear wave-wave interactions (due to quadruplets and triads), generation by wind and dissipation (due to white-capping, bottom friction and depth-induced breaking).

Bathymetry

Bathymetries for the $500m$ wave and flow grids were created, and were as shown in continuous filled contours in Figures 5 and 6. The legend in Figure 5 shows the topology on land in yellow with negative values (positive being under water level). The legend in Figure 6 shows the topology on land in green with negative or zero values.

VALIDATION

The models developed can only be employed to perform predictive simulations only after thorough validation against measured physical system data. The location of the IPOSS buoy and ADCP of which wave and flow data respectively were collected and used to calibrate these numerical models are shown in Figure 1.

Wave model validation

The numerical model was set up to run for a time period from 1 January 2013 to 1 May 2013 and calibrated at an output point at latitude: -33.822528° and longitude: 25.692778° which is the location of the IPOSS waverider buoy. The buoy collected wave data for the set time period and the data were used to calibrate the wave model. Figures 7, 8 and 9 show plots of significant wave height, wave direction and peak wave period respectively at model output corresponding to the IPOSS buoy location. Boundary conditions used to force the model were obtained from NCEP1 (32565) located at latitude: -35.000000° and longitude: 26.250000°. This model was considered satisfactory given that it captures the recorded data reasonably well.

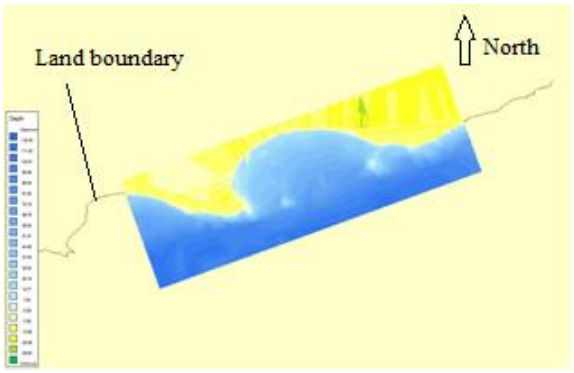

Figure 5 Bathymetry for the wave grid model with a 500m grid resolution for the Algoa Bay.

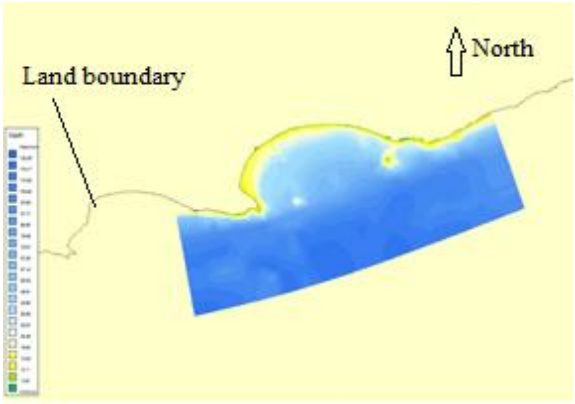

Figure 6 Bathymetry for the flow grid model.

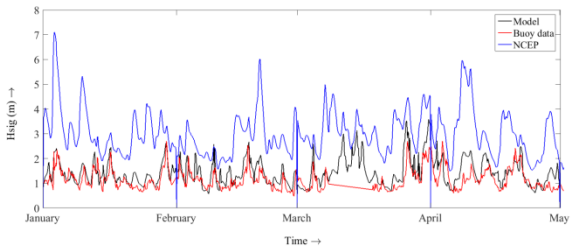

Figure 7 Significant wave height plot of model and IPOSS buoy data together with the NCEP conditions applied at the model boundary for the period 1 January 2013 to 1 May 2013.

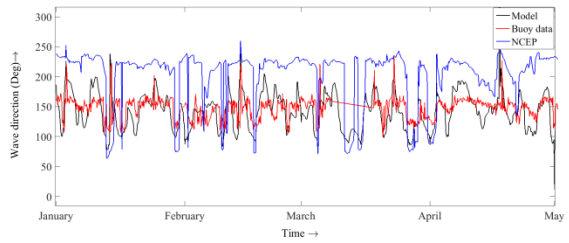

Figure 8 Wave direction plot of model and IPOSS buoy data together with the NCEP conditions applied at the model boundary for the period 1 January 2013 to 1 May 2013.

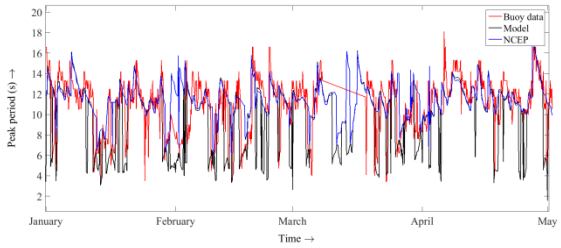

Figure 9 Peak wave period plot of model and IPOSS buoy data together with the NCEP conditions applied at the model boundary for the period 1 January 2013 to 1 May 2013.

Flow model validation

The time period between 1 March 2013 and 1 May 2013 were used for validation of the flow model. Figures 10 and 11 show plots of x and y components of the depth averaged velocity at a selected model output location. The model outputs were compared to data from the ADCP moored at a latitude and longitude -34.0074° and 25.72034° respectively which is on Bird Island. This ADCP data was made available courtesy of the South African Environmental Observation Network (SAEON).

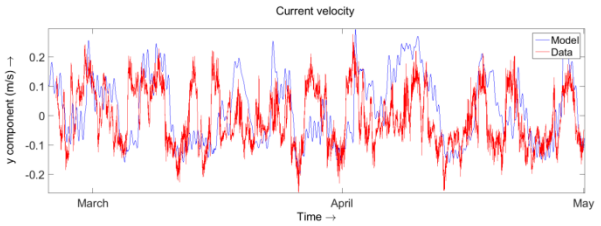

Figure 10 Y components of depth average velocity model output compared with ADCP data for the period 1 March 2013 to 1 May 2013.

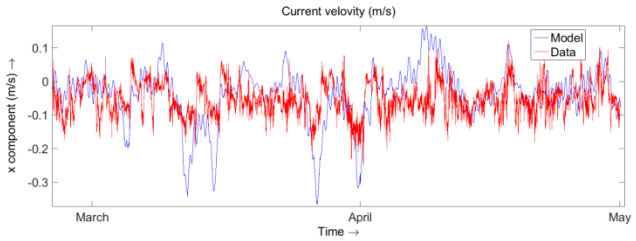

Figure 11 X components of depth average velocity model output compared with ADCP data for the period 1 March 2013 to 1 May 2013.

RESULTS AND DISCUSSION

Two simulations with the sediment bypass systems modelled and without one were ran both starting from the 1st of January 2013 to 1st of July 2013. The results from the two simulations are compared and discussed below. The two simulations were started at 03:00:00, 1 January 2013. In order to analyse the effects of the waves, current and wave-induced flow on the sediment transport on the sea bed we looked at the accumulation or erosion of sediment in whole modelling domain with time. The colour scales of filed contours in Figure 12 were clipped at $-3m$ and $+3m$. Picture (a) and picture (b) in Figure 12 show the state of the sea bed for the simulation with a bypass system and one without, respectively, at 15:00:00, 1 January 2013. For both simulations there is zero net accumulation/erosion evident. However when the simulated time has moved to 15:00:00, 1 July 2013 picture (c) for the bypass system and picture (d) without one, in Figure 12, show accumulation and erosion of sediment along the coastline and surf zone. From Figure 12 it is evident that the simulation with a bypass system has higher rates of accumulation and erosion of sediment as illustrated by wider areas of coloured in blues and red shades. Figure 12 shows the effects a man-made system can have on speeding up the natural sediment transport process along the coast line of a bay as it removes sediment in the surf zone and depositing it a few kilometres offshore.

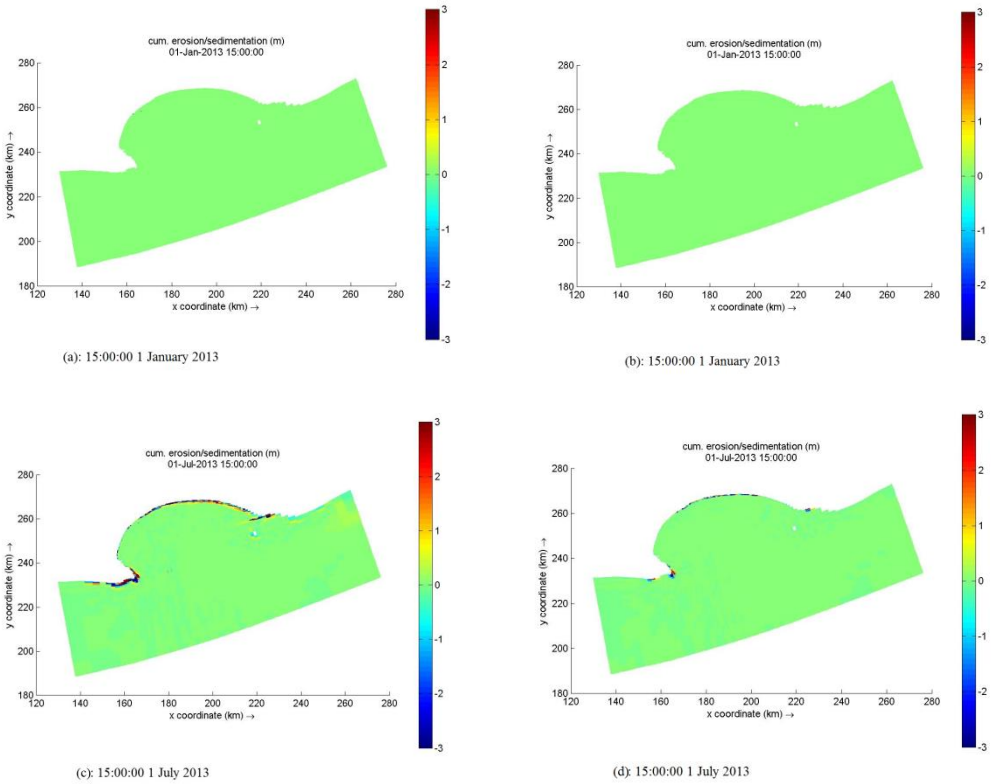

Figure 12 Plots of accumulation and erosion (m) showing time series snap shots of filled contours for simulations with a Sediment bypass system (pictures (a) and (c)) and one without (pictures (b) and (d)).

The forces responsible for the sediment transport that is mostly concentrated in the surf zone are dominated by wave induced forces. These wave induced forces are a consequence of a phenomenon called wave steepness whereby wave crests have a higher amplitude than the wave troughs, which results in a net onshore force. The time series progression of the magnitude of the wave induced forces and the location of where there are dominant are plotted in Figure 13. It is illustrated in Figure 13 that most of the wave induced forcing takes places along the surf zone because the ocean depth is shallow, which leads to wave refraction of the sea bed. The wave induced forces are also strong in regions that are a distance from the surf zone, but this is due to the fact the depth at those locations is also shallow, thereby resulting in wave refraction. The wave induced forces generated for the bay with a bypass system seem to be similar to those generated in bay without a bypass system as illustrated in Figure 13 The wave spectra responsible for the wave induce forces are plotted in Figure 14, where the time series progression of the wave significant height is shown. Both the significant wave height and mean significant wave direction vector are plotted to show the size of waves that come into the bay and the extent of refraction the waves experience from the ocean bed as they progress into the bay.

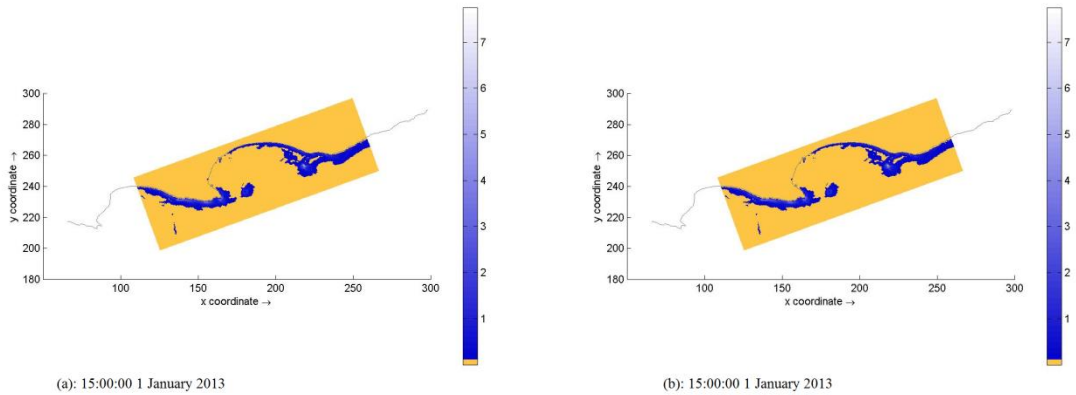

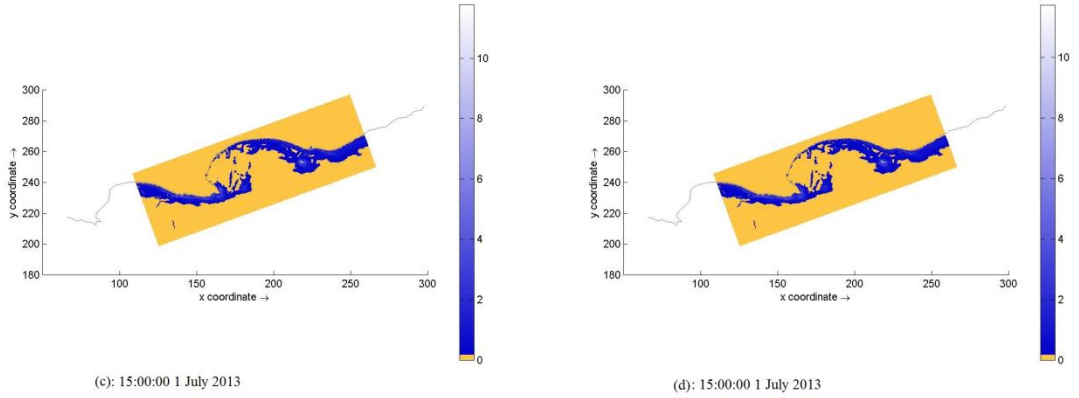

Figure 13 Plots of the magnitude of the wave induced forces (N/m^2) showing time series snap shots of filled contours for simulations with a sediment bypass system(pictures (a) and (c)) and one without (pictures (b), and (d)).

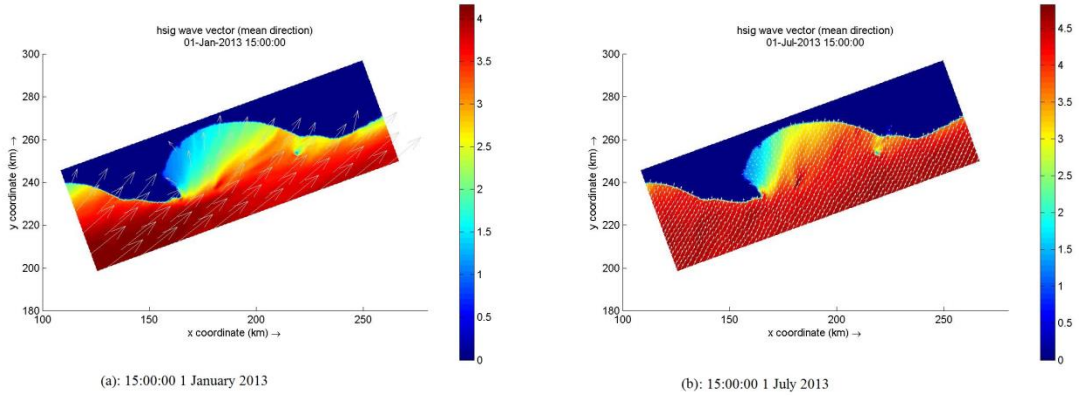

Figure 14 Plots of the significant wave height (m) filled contours and direction vector showing time series snap shots for simulations with a sediment bypass system or without (pictures (a) and (b)).

Essentially the waves originate in the southern ocean and come from the south and south-eastern direction. As the sediment accumulates and erode in different places on the ocean bed the bathymetry of the ocean bed changes, which in turn affects how the water near the ocean bed flow. This effect of the bathymetry is illustrated in Figure 15 where there is a marked difference in the time series progression of the water velocity field near the ocean bed for the bay with a bypass system and the bay without a bypass system. Figure 15 shows the water velocity magnitude together with the velocity direction vector.

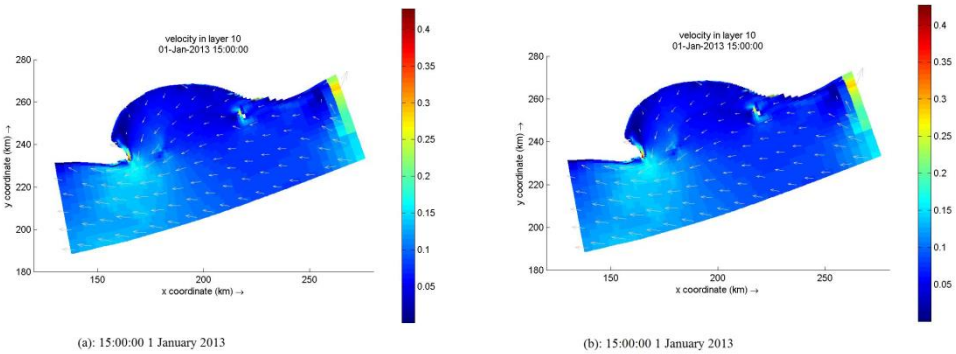

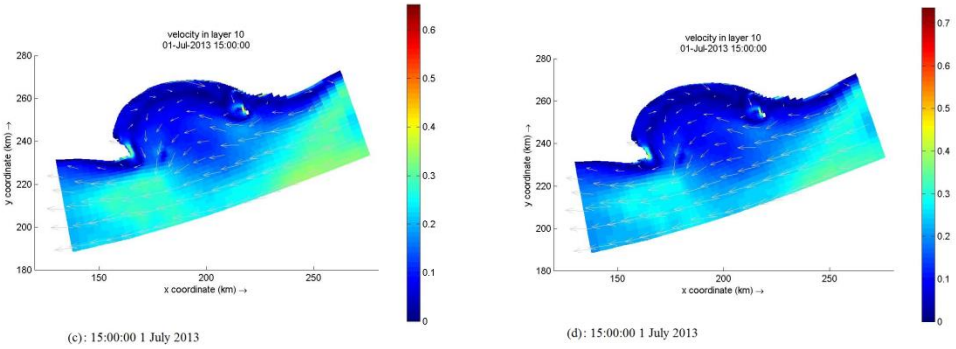

Figure 15 Plots of the near bed flow velocity magnitude filled contours and direction vector(m/s) showing time series snap shots for simulations with a sediment bypass system(pictures (a) and (c)) and one without (pictures (b) and (d)).

CONCLUSIONS

The results from the numerical simulations show that the blockage of the bypass system, which is represented by the simulation without a bypass system will result in less sediment movement across the bay. That is the sediment transport observed is due solely to the natural sediment transport eastwardly. However if the sediment bypass system is functioning properly the sediment transport rate is enhanced greatly, thereby negating the need to dredge the entrance channel into the Port of Ngqura.

ACKNOWLEDGEMENTS

The authors of the paper would like to express their gratitude to the National Research Foundation (NRF) of South Africa for their financial support in funding the conference travel expenses.

REFERENCES

[1] Schumann E.H., Brink K.H., Coastal-trapped waves off the coast of South Africa: Generation, propagation and current structures. *Journal of Physical Oceanography*. Vol. 20, 1990, pp. 1206-1218.

[2] Goschen, W. S., Schumann, E. H., Bernard, K. S., Bailey, S. E., Deyzel, S. H. P., Upweling and ocean structures off Algoa Bay and the south-east coast of South Africa. *African Journal of Marine Science*. Vol. 34(4), 2012, pp. 525-536.

[3] Roberts M.J., Coastal currents and temperatures along the eastern region of Algoa Bay, South Africa, with implications for transport and shelf-bay water exchange, *African Journal of Marine Science*, Vol. 32(1), 2010, pp. 145-161.

[4] Lwandle, Port of Ngqura Marine Infrastructure Development EIA: Marine Ecology Specialist study, *Lwandle Report No LT 165*, 2013.

[5] Goschen W.S., Schumann, E. H., The physical oceanographic processes of Algoa Bay, with emphasis on the western coastal region. *SAEON internal publication*, 2011.

[6] Schumann E. H. and Martin J. A., Climatological aspects of the coastal wind field at Cape Town, Port Elizabeth and Durban. *South African Geographical Journal*, Vol. 73, 1991, pp. 48-51.

[7] Goschen, W.S. and Schumman E.H., The physical oceanogcal oceanographic processes of Algoa Bay, with emphasis on the western coastal region, *SAEON/IMT internal publication, IMT Document number: P0106-110000-730002*, 2010.

[8] Theron AK, Rossouw M, Rautenbach C, Von Saint Ange U, Maherry A and August M., Determination of Inshore Wave Climate along the SA coast - Phase 1 for Coastal Hazard and Vulnerability Assessment. *CSIR Report ECCS082*, Stellenbosch, South Africa. 2013.

[9] Deltares, Delft3D-Wave User Manual – Simulation of short-crested waves with SWAN, *Part of Hydro-morphodynamics (Version 3.04, Rev. 15779)*, Deltares, Delft. The Netherlands, 2011.

[10] Deltares, Delft3D-FLOW User Manual – Simulation of multi-dimensional hydrodynamic flows and transport phenomena, including sediments, *Part of Hydro-morphodynamics (Version 3.15, Rev. 18392), Deltares*, Delft. The Netherlands, 2011.